

Observations of nearshore circulation: Alongshore uniformity

Falk Feddersen

Woods Hole Oceanographic Institution, Woods Hole, Massachusetts, USA

R. T. Guza

Scripps Institution of Oceanography, La Jolla, California, USA

Received 9 January 2002; revised 2 August 2002; accepted 28 August 2002; published 4 January 2003.

[1] Nearshore circulation, observed for 4 months on a 200-m-long stretch of natural beach during the SandyDuck field experiment, is shown to be alongshore uniform. An alongshore momentum balance between (wind and wave) forcing and bottom stress, cross-shore integrated between the shoreline and approximately 4 m water depth, holds on each of five instrumented cross-shore transects (skill ≥ 0.87). The corresponding five best fit drag coefficients are similar, consistent with the assumption that terms in the momentum balance associated with alongshore nonuniformity are negligible. In addition, the alongshore nonuniformity of the circulation and bathymetry were examined at five cross-shore locations. Except near the shoreline, the circulation and bathymetry were rarely strongly alongshore nonuniform, and the circulation nonuniformities were usually no larger than expected from current-meter noise alone. Near the shoreline, the bathymetry was more irregular and the circulation was often detectably nonuniform, although no relationship between bathymetric and circulation nonuniformities was found. The closure of the alongshore momentum balances on cross-shore transects, and the observed alongshore uniformity of the circulation on four of five alongshore transects, demonstrates that the simplified dynamics of alongshore uniform circulation are valid during the experiment. *INDEX TERMS*: 4546 Oceanography: Physical: Nearshore processes; 4219 Oceanography: General: Continental shelf processes; 4512 Oceanography: Physical: Currents; *KEYWORDS*: circulation, SandyDuck, oceanography, nearshore, bathymetry

Citation: Feddersen, F., and R. T. Guza, Observations of nearshore circulation: Alongshore uniformity, *J. Geophys. Res.*, 108(C1), 3006, doi:10.1029/2001JC001293, 2003.

1. Introduction

[2] The assumption that nearshore bathymetry, waves, and currents are alongshore uniform simplifies the governing equations for the circulation. The depth- and time-averaged alongshore momentum equation reduces to a one-dimensional (1-D) balance between wind and wave forcing, bottom stress, and lateral mixing [i.e., *Longuet-Higgins*, 1970]

$$\tau_y^{\text{wind}} - \frac{dS_{yx}}{dx} = \tau_y^b + \frac{dM_{yx}}{dx}, \quad (1)$$

where x and y are the cross- and alongshore coordinates, respectively. The alongshore wind stress is τ_y^{wind} , wave-forcing is given by the cross-shore gradient of S_{yx} (the off-diagonal component of the wave radiation stress tensor), τ_y^b is the time-averaged alongshore bottom stress, and mixing is represented by the cross-shore gradient of the depth-integrated turbulent momentum flux (or Reynolds stress) M_{yx} . For alongshore uniform conditions, these terms vary only in the x direction.

[3] No beach bathymetry, wave field, or nearshore circulation is exactly alongshore uniform, but good agreement between 1-D alongshore current model (1) predictions and observations suggested that the effects of nonuniformities were weak on the nonbarred and qualitatively alongshore uniform bathymetry at Santa Barbara during the 1980 NSTS experiment [e.g., *Thornton and Guza*, 1986]. However, the suggested reasons for the 1-D model-data disagreement on the barred beach at Duck N. C. during the 1990 DELILAH experiment [*Church and Thornton*, 1993] have included violation of the 1-D assumption [*Reniers et al.*, 1995]. The statistical closure of the cross-shore integrated 1-D alongshore momentum balance (1), estimated from a single cross-shore transect at Duck N. C. during the Duck94 experiment, demonstrated that the integrated 1-D dynamics held for the wide range of nearshore conditions, although some cases were presented where the circulation and dynamics must have been two-dimensional (2-D) [*Feddersen et al.*, 1998]. The cross-shore variation of mean alongshore currents observed on two barred beaches (the 1998 Coast3D experiment at Egmond, Netherlands and Duck94) agreed reasonably well with 1-D model predictions for approximately 2/3 of each experiment period when the bathymetry was most alongshore uniform [*Ruesink et al.*, 2001]. The disagreement during the other 1/3 of

each experiment period was ascribed to 2-D effects associated with increased alongshore bathymetric nonuniformities. In these studies, the alongshore uniformity or nonuniformity of the circulation was inferred. Direct observations of alongshore variability were limited because mean currents were measured primarily on a single cross-shore transect.

[4] Here, observations from an extensive 2-D array of instruments (section 2) are used to investigate the alongshore nonuniformity of the nearshore circulation. Alongshore current dynamics are investigated in section 3. Cross-shore integrated 1-D alongshore momentum balances based on (1) close at five alongshore locations separated by up to 200 m. The inferred drag coefficients are (statistically) indistinguishable, indicating that there are no unaccounted for sources or sinks of momentum over the 200-m long alongshore span, and that cross-shore integrated 1-D dynamics are valid. The local (at a particular cross-shore location) validity of the 1-D assumption is investigated kinematically by inspecting the deviation from alongshore uniform circulation (section 4). Except near the shoreline, circulation nonuniformities rarely were greater than expected from current-meter noise alone. No systematic relationship between bathymetric and circulation nonuniformities near the shoreline was found. A rip-current example, an exception to the usual alongshore uniform circulation, also is discussed.

[5] The conclusion from the dynamical and kinematic analyses is that, for the conditions encountered, the observed circulation is often alongshore uniform everywhere (section 5). Thus, a model that incorporates the 1-D dynamics of wave and wind-forcing, lateral mixing, and bottom stress is in principle capable of accurately modeling the alongshore current during most of the experiment period.

2. Observations

[6] The data discussed here were collected from 3 August through 21 November 1997 during the SandyDuck field experiment, conducted near Duck, North Carolina on a barrier island exposed to the Atlantic Ocean. Directional properties of the incident wave field were estimated from a 2-D array of 15 bottom-mounted pressure sensors in 8-m depth, approximately 750-m from the shoreline [Long, 1996]. Wind speed and direction measured 19.5 m above mean sea level at the end of a nearby pier were used to estimate wind stress using the algorithm of *Large and Pond* [1981]. Bathymetry surveys that spanned roughly 450 m in the cross-shore (nominally to 6-m depth) and 500 m in the alongshore were obtained at least once a week during the first 90 days of the experiment.

[7] Colocated sonar altimeters, pressure sensors, and bidirectional electromagnetic current-meters were deployed in a 2-D array spanning 225 m and 200 m in the cross- and alongshore, respectively (Figure 1). Five cross-shore transects with five instrumented locations that span from $x = 20$ m to $x = 245$ m (approximately 4 m depth) are denoted C1 to C5 (Figure 1). Five alongshore transects, located at $x = 20, 70, 120, 170,$ and 245 m, each with five instrumented locations are denoted A1 to A5 (Figure 1). The alongshore spacing between current-meters ranges between 28 m and 200 m.

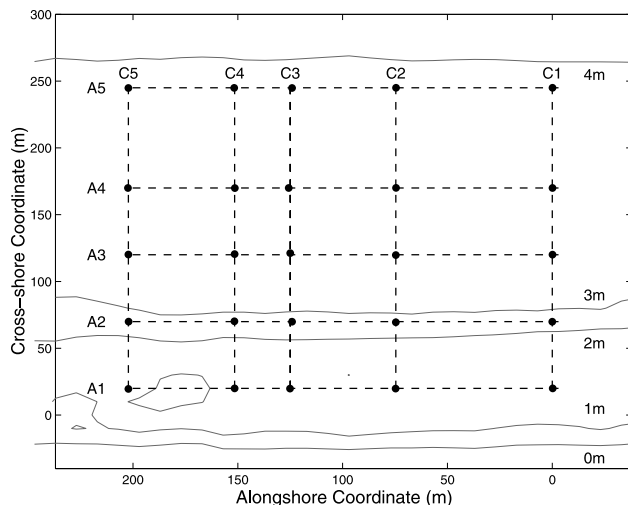


Figure 1. Locations (circles) of the instrumented frames. Bathymetry from 2 October (day 60) is contoured in units of meters below mean sea level. The coordinate system orientation of the U.S. Army Corp of Engineers Field Research Facility (FRF) is used; x increases offshore and y increases in approximately the northerly direction. The origin of the present coordinate system corresponds to FRF coordinates $x = 140$ m and $y = 703$ m. The alongshore and cross-shore transects are denoted A1–A5 and C1–C5, respectively.

[8] Current-meter offset drift was accounted for by regularly rotating the current-meters 180° and assuming a stationary mean current during approximately 10-min periods before and after rotation. Biofouling required repeated cleaning of the current-meter probes. Data from heavily biofouled current-meters or with possibly large offset-drift-induced errors were discarded. The most onshore sensors often were exposed at low tide and therefore inactive. The current-meters were raised or lowered as the bed level changed to maintain an elevation usually between 0.4 m and 1.0 m above the seafloor. Pressure sensor, current-meter, and altimeter data acquired at 2 Hz were processed into hourly averages.

[9] Conditions during the experiment are summarized in Figure 2. In 8-m depth, the range of incident wave properties was; root-mean square (rms) wave height H_{rms} (0.15 to 2.7 m, Figure 2a), mean (energy-weighted) wave frequency (0.08 to 0.24 Hz), mean wave angle θ (-47° to 58° , positive angles correspond to waves from the north), and the directional spread (12° to 68°). Strong alongshore winds, large obliquely incident waves, and strong alongshore currents often coincided. In 8-m depth, $-S_{yx}/\rho$ (ρ is the constant water density) estimated with a directional-moment technique [Elgar *et al.*, 1994], ranged between -0.5 to 0.8 m^3/s^2 (Figure 2b), and is correlated ($r^2 = 0.58$) with the alongshore wind stress τ_y^{wind} (Figure 2c). The maximum observed mean alongshore current \bar{v}_{max} varied between 1.4 and -1.7 m/s (Figure 2d), was most often located on the A1 transect closest to shore, and was correlated ($r^2 = 0.79$) with $-S_{yx}/\rho$. The observed range of \bar{v} magnitudes is similar to previous observations at Duck [e.g., Church and Thornton, 1993;

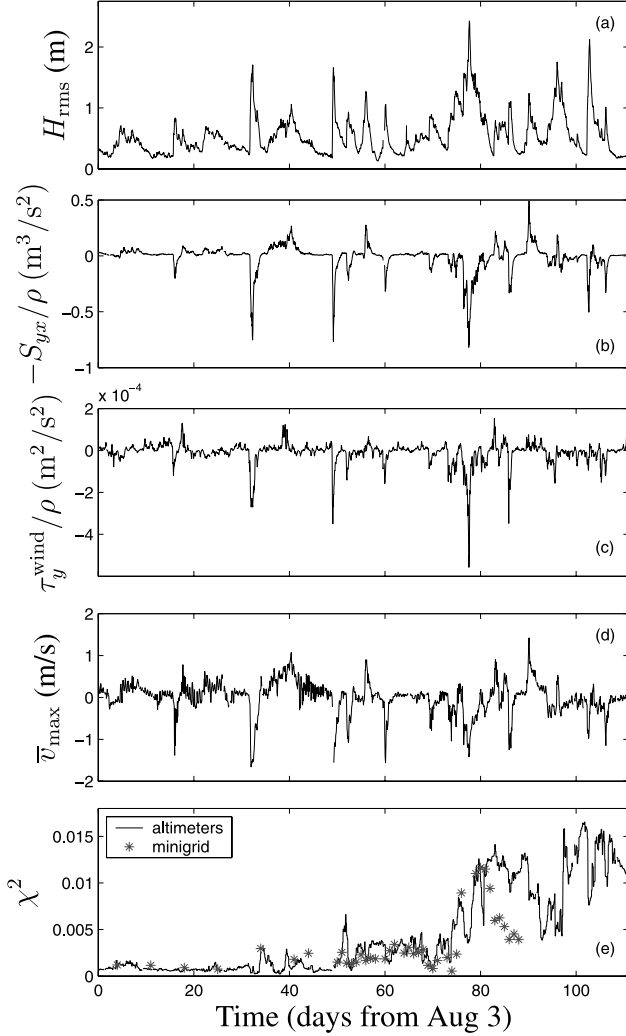


Figure 2. Time series of (a) H_{rms} and (b) $-S_{yx}/\rho$ at the 8-m array, (c) τ_y^w/ρ , (d) \bar{v}_{max} , and (e) χ^2 the measure of bathymetric nonuniformity (2). Positive $-S_{yx}/\rho$, τ_y^w/ρ , and \bar{v}_{max} correspond to waves, wind, and mean alongshore currents from the south. Values of $\chi^2(2)$ calculated from altimeters and bathymetric surveys agree well until day 80.

Feddersen et al., 1996], as is the correlation between \bar{v}_{max} and $-S_{yx}$ [*Feddersen et al.*, 1998].

[10] The alongshore uniformity of the bathymetry within the 2-D instrumented array is characterized by the metric χ^2 [*Ruessink et al.*, 2001], defined as

$$\chi^2 = \frac{1}{L_x L_y} \int_0^{L_x} \int_0^{L_y} \left(\frac{h(x,y) - \bar{h}(x)}{\bar{h}(x)} \right)^2 dy dx, \quad (2)$$

where $h(x, y)$ is the mean water depth relative to mean sea level, $\bar{h}(x)$ is the alongshore-transect integral-averaged depth, and $L_x = 225$ m and $L_y = 200$ m represent the cross- and alongshore integration distances, respectively. In late October (around day 80), χ^2 increased to about 0.015 as bathymetric irregularities developed at the north end of the instrumented region (Figure 2e).

[11] The cross-shore integration in (2) can obscure local bathymetric nonuniformities, and their potential effect on the circulation. Local bathymetric nonuniformities are characterized by two statistics, the alongshore depth variance $\sigma_h^2(x)$ (or standard deviation σ_h) defined as,

$$\sigma_h^2(x) = \frac{1}{L_y} \int_0^{L_y} (h(x,y) - \bar{h}(x))^2 dy, \quad (3)$$

and mean depth normalized variance γ^2 defined as,

$$\gamma^2(x) = \frac{\sigma_h^2(x)}{\bar{h}^2(x)}. \quad (4)$$

Altimeter estimates of χ^2 , σ_h and γ^2 are used below.

[12] The time (over the entire 4 months) mean and standard deviation of the depth statistics are given in Table 1. On average, the depth at A2 is 1.6 m deeper than at A1, and the \bar{h} range at A2 (2.35–3.15 m) is the largest of all the transects. The σ_h depth nonuniformity is about the same at A2 as at A1, but due to the increased depth at A2, γ^2 is on average 20% of γ^2 at A1. Farther offshore at A3–A5, \bar{h} increased to between 3.4 and 3.9 m, the \bar{h} temporal variability decreased, and the bed was much more alongshore uniform than at A1–A2 (Table 1).

3. Circulation Dynamics

[13] Assuming alongshore uniform (1-D) and steady ($\partial_t = 0$) circulation, the time- and depth averaged alongshore momentum equation (1) is [e.g., *Longuet-Higgins*, 1970],

$$\rho^{-1} \left(\tau_y^w - \frac{dS_{yx}}{dx} \right) = c_d \langle |\bar{u}|v \rangle + \rho^{-1} \frac{dM_{yx}}{dx}. \quad (5)$$

The mean alongshore bottom stress τ_y^b/ρ is represented by the product of the nondimensional drag coefficient c_d and the quadratic velocity moment $\langle |\bar{u}|v \rangle$, where $\langle \cdot \rangle$ represents a time average over many wave periods. The horizontal velocity vector \bar{u} and the alongshore velocity v include both mean and wave components, above the bottom boundary layer.

[14] The 1-D alongshore current dynamics are not verified locally (5) because it is difficult to estimate accurately the S_{yx} and M_{yx} gradients. However, cross-shore integrated 1-D alongshore current dynamics can be tested with a cross-shore transect of observations [*Feddersen et al.*, 1998].

Table 1. Time Mean and Standard Deviation of Bathymetry Statistics on Alongshore Transects A1–A5^a

	\bar{h} , m		σ_h , m		γ^2	
	Mean	Standard Deviation	Mean	Standard Deviation	Mean	Standard Deviation
A1	1.22	0.14	0.18	0.12	0.0275	0.0277
A2	2.84	0.20	0.15	0.14	0.0057	0.0102
A3	3.63	0.07	0.07	0.02	0.0004	0.0002
A4	3.47	0.04	0.05	0.01	0.0002	0.0001
A5	3.86	0.08	0.04	0.01	0.0001	0.0001

^aThe depth \bar{h} is relative to the mean sea level, and σ_h and γ^2 are defined in (3) and (4), respectively.

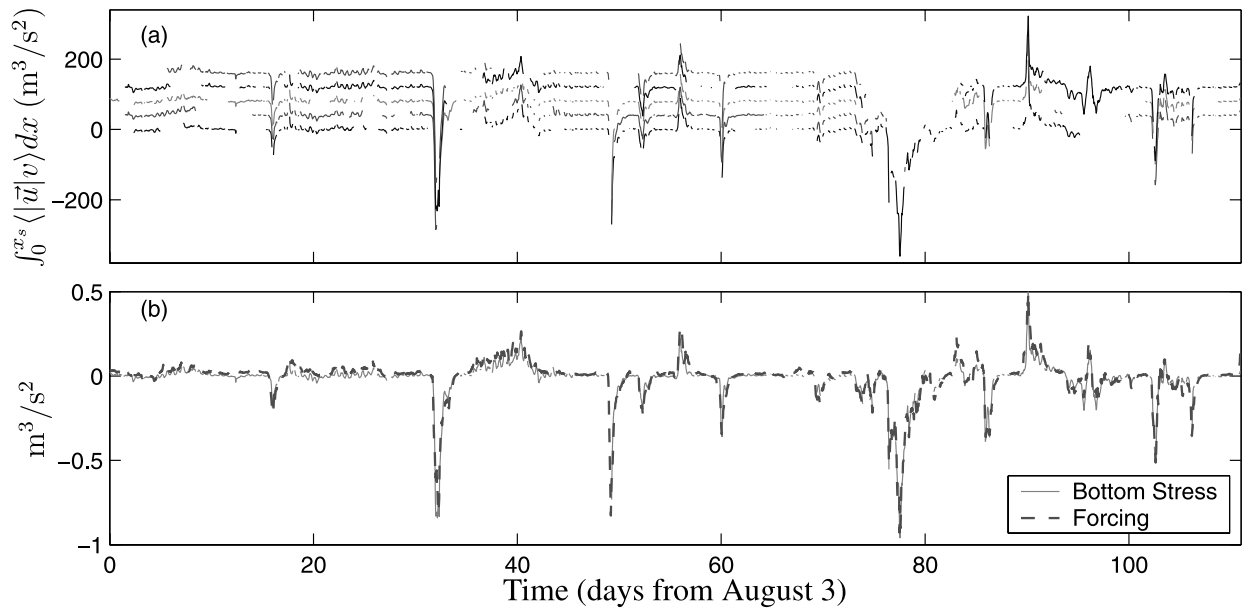


Figure 3. (a) $\int_0^{x_s} \langle |\bar{u}|v \rangle dx$ from the C1–C5 cross-shore transects versus time. Each transect is offset by increments of 40 m^3/s^2 . (b) Along-shore averaged cross-shore integrated bottom stress (solid) and (wind + wave) forcing (dashed) versus time. Statistics are presented in Table 2.

Wave breaking rarely occurred (about 3% of the time) between 8-m depth ($x = 750$ m) where S_{yx} was estimated, and the offshore end ($x_s = 225$ m) of the cross-shore transects. Therefore, by linear theory on the approximately parallel depth contours, S_{yx} is conserved between 8-m depth and the offshore end of the transects. The Reynolds stress M_{yx} is assumed negligible at the offshore end of the transect. Based on the assumption that momentum sources and sinks onshore of A1 are negligible in the integrated (over 225 m) momentum balance, both S_{yx} and M_{yx} are assumed zero at $x = 0$. Although c_d varies in the cross-shore [Feddersen *et al.*, 1998; Ruessink *et al.*, 2001], it is passed through the integral and interpreted as a spatially averaged c_d (Appendix A). With a spatially constant wind stress, the cross-shore integral of (5) becomes

$$\frac{\tau_y^{\text{wind}}}{\rho} x_s - \frac{S_{yx}}{\rho} \Big|_{x_{\text{sm}}} = c_d \int_0^{x_s} \langle |\bar{u}|v \rangle dx, \quad (6)$$

where x_s is the transect length (225 m). The $\int_0^{x_s} \langle |\bar{u}|v \rangle dx$ time series is estimated on each transect (Appendix B) and c_d is considered an unknown. The balance (6) is tested statistically on each transect using linear regression (least squares), yielding the momentum balance skill r^2 , best fit c_d , and c_d uncertainty (standard deviation) σ_{c_d} (Appendix B).

[15] Due to data gaps, $\int_0^{x_s} \langle |\bar{u}|v \rangle dx$ was calculated for different time periods on each transect ranging between 790 (C5) and 1404 (C4) hours out of 2664 possible hours. The $\int_0^{x_s} \langle |\bar{u}|v \rangle dx$ time series for all transects were similar (Figure 3a) indicating that $\int_0^{x_s} \langle |\bar{u}|v \rangle dx$ was alongshore uniform. Using the alongshore averaged (over C1–C5) $\int_0^{x_s} \langle |\bar{u}|v \rangle dx$ (denoted AVG in Table 2, calculated for 2132 hours), the integrated momentum balance (6) closed with high skill (Figure 3b, $r^2 = 0.92$) and best fit $c_d = 2.66 \pm 0.07$ ($\times 10^{-3}$), similar to the Duck94 integrated momentum balance [Fed-

dersen *et al.*, 1998]. The cross-shore integrated alongshore momentum balance is dominated by wave-forcing; the RMS wave-forcing is 10 times larger than the RMS wind-forcing. The balance (6) also closed on each individual cross-shore transect (C1–C5) with high skill ($r^2 > 0.87$), best fit c_d between 2.40 and 3.02 ($\times 10^{-3}$), and uncertainty σ_{c_d} between 0.11 and 0.18 ($\times 10^{-3}$) (Table 2). If the true $c_d = 2.7 \times 10^{-3}$ and $\sigma_{c_d} = 0.15 \times 10^{-3}$, then all c_d estimates (Table 2) are similar, within $2\sigma_{c_d}$ of the true value. The high skill and similar c_d on all transects suggests that no sources or sinks of cross-shore integrated alongshore momentum are neglected in (6), and that alongshore uniform (1-D) dynamics are valid over the array. The closures do not necessarily imply that the 1-D momentum balance holds locally (5), because 2-D terms (e.g., nonlinear and alongshore pressure gradient) could be locally strong, but change sign with cross-shore location such that their cross-shore integrals cancel. However, consistent cancellation seems unlikely to occur over the wide range of bathymetric and forcing conditions encountered during the 4-month-long experiment. In addition, the maximum χ^2 of 0.015 is less than the level ($\chi^2 > 0.02$) of bathymetric nonuniformity observed by Ruessink *et al.* [2001] to induce circulation nonuniformities.

Table 2. Statistics of the Cross-Shore Integrated Momentum Balances^a

Transect	N	r^2	$c_d \pm \sigma_{c_d}$ ($\times 10^{-3}$)
C1	930	0.94	2.77 \pm 0.11
C2	1141	0.87	2.60 \pm 0.15
C3	1091	0.89	3.02 \pm 0.15
C4	1405	0.89	2.40 \pm 0.11
C5	790	0.87	2.45 \pm 0.18
AVG	2132	0.92	2.66 \pm 0.07

^a N is the number of hours in the balance, r^2 is skill of the balance (5) and c_d and σ_{c_d} are the best-fit and standard deviation of the drag coefficient, respectively.

[16] The neglected acceleration term in the cross-shore integrated 1-D alongshore momentum balance (6)

$$\frac{d}{dt} \left[\int_0^{x_s} h \bar{v} dx \right], \quad (7)$$

was estimated on each transect (Appendix B). This term is small, 6–8% of the wave forcing, and is not correlated with $\int_0^{x_s} \langle |\bar{u}| \bar{v} \rangle dx$ ($r^2 < 0.03$) because it contains variability on timescales much shorter than the forcing or bottom stress variability. Thus, the estimates of (7) likely are dominated by noise, consistent with previous results [Feddersen *et al.*, 1998; Lentz *et al.*, 1999] that the circulation on hourly timescales is in equilibrium with the forcing and that acceleration terms are negligible.

[17] The 1-D balance (5) is tested further by examining the size of the neglected, cross-shore integrated, nonlinear advection term

$$\frac{d}{dy} \left[\int_0^{x_s} h \bar{v}^2 dx \right], \quad (8)$$

estimated between alongshore transect pairs (Appendix B). This term was large, of the same order of magnitude as the total forcing, but decreased in magnitude approximately inversely with increasing transect spacing Δy (Figure 4). This decrease is consistent with simulations of (8) based on alongshore uniform mean currents and depths (from observations) and superimposed Gaussian current-meter noise (Figure 4). Thus, although (8) could be nonzero and dynamically important to the circulation, the observed (8) also are consistent with being solely due to current-meter noise. If (8) were important, then either the 1-D momentum balances would not close well or there would be significant transect to transect variation of c_d , neither of which was observed.

4. Circulation Kinematics

[18] Although the cross-shore-integrated, alongshore current dynamics are alongshore uniform, local (at a particular cross-shore location) alongshore nonuniformities in the circulation could still be present but either cancel or contribute little to the integrated balance. The local validity of the 1-D assumption could not be investigated dynamically, so the nonuniformity of the circulation instead is investigated kinematically. Alongshore nonuniformities of \bar{v} and \bar{u} on each alongshore transects (A1–A5) are characterized with the maximum deviation ($|\delta\bar{v}|_{\max}$ and $|\delta\bar{u}|_{\max}$) from the alongshore-transect mean (\bar{v} and \bar{U}), and the maximum deviation normalized by the mean current ($|\delta\bar{v}|_{\max}/|\bar{v}|$ and $|\delta\bar{u}|_{\max}/|\bar{U}|$). The observed deviations from uniformity and the current-meter noise threshold curves (Appendix C) are shown in Figure 5 as functions of $|\bar{v}|$ and $|\bar{U}|$.

4.1. Alongshore Current

[19] At the most onshore alongshore transect A1, the \bar{v} alongshore nonuniformity often (between 25% and 50% of the time) exceeded that expected from current-meter noise alone for all $|\bar{v}|$ (Figure 5a; Table 3). However, \bar{v} was sometimes remarkably uniform with less than 10% variation from the transect average $|\bar{v}|$. Transect A1 had the largest $|\bar{v}|$

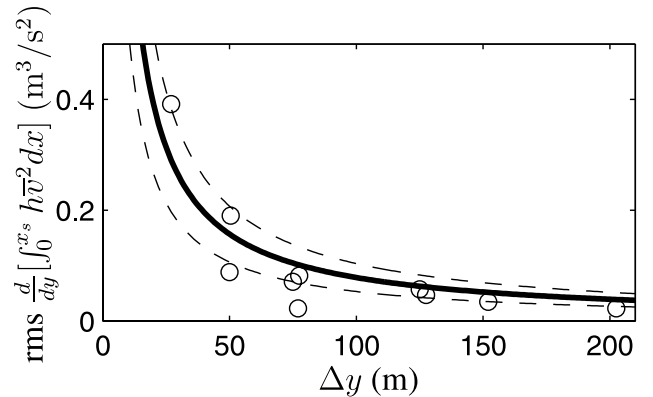


Figure 4. Root-mean square values of (8) versus the separation between transect pairs Δy . The open circles are observations. The solid (dashed) curve represent mean (\pm one standard deviation) RMS simulated estimates of alongshore uniform (8) based on the observations and a superimposed zero-mean Gaussian (standard deviation 0.04 m/s, 24 hr decorrelation time) current-meter noise. Varying the decorrelation time between 6 hours to 8 days does not affect the results.

range, reaching 1.6 m/s, with $|\bar{v}| > 0.4$ m/s about 21% of the time. For these cases with strong currents, 29% of the time $|\delta\bar{v}|_{\max}/|\bar{v}| > 0.2$, and the largest $|\delta\bar{v}|_{\max}/|\bar{v}|$ was 1.1. No difference in $|\delta\bar{v}|_{\max}/|\bar{v}|$ was observed with northward or southward current at A1, nor at any other transect (A2–A5), suggesting that \bar{v} nonuniformities are not caused by some persistent larger scale feature outside the instrumented region, such as the pier located at $y = -200$ m [Elgar *et al.*, 2001]. Fifty meters farther offshore at A2, $|\bar{v}|$ was weaker, never exceeding 1.0 m/s (Figure 5b), and $|\bar{v}| > 0.4$ m/s only about 6% of the time. The \bar{v} at A2 was more uniform than at A1, at times exceeding the noise thresholds (Table 3). Farther offshore at A3, A4, and A5, the maximum $|\bar{v}|$ was larger than at A2, reaching 1.6 m/s, but $|\bar{v}| > 0.4$ m/s only about 5% of the time (Figures 5c and 5d). At A3, A4 and A5, where waves often were not breaking, \bar{v} was more uniform than at either A2 or A1 (Table 3), and the nonuniformity is not larger than expected for current-meter noise alone.

[20] One of the largest observed A1 nonuniformities and the characteristically uniform flow farther offshore is shown in Figure 6. At A1, $|\bar{v}| = 0.91$ m/s and $|\delta\bar{v}|_{\max}/|\bar{v}| = 0.44$ (circle in Figure 5a). The nonuniformity occurs at the southern A1 current-meter ($y = 0$ m) where \bar{v} was 0.5 m/s less than observed at the other three current-meters (which differed from each other by only 0.03 m/s). This nonuniform circulation pattern at A1 was observed for approximately 36 hours, accounting for many of the nonuniform cases adjacent to the circle in Figure 5a. Farther offshore at A2–A5, \bar{v} was weaker than at A1, and the alongshore nonuniformity of \bar{v} did not exceed either noise threshold (compare circles in Figures 5b–5d with the circle in 5a).

[21] From the altimeters, the water depth was only 0.1 m deeper at the location of the nonuniform current, a relatively small depth nonuniformity (0.18 m is the mean depth nonuniformity on A1, Table 1). The wave height also was approximately alongshore uniform, with H_{rms} varying between 0.44 and 0.47 m on A1 and between 0.88 and

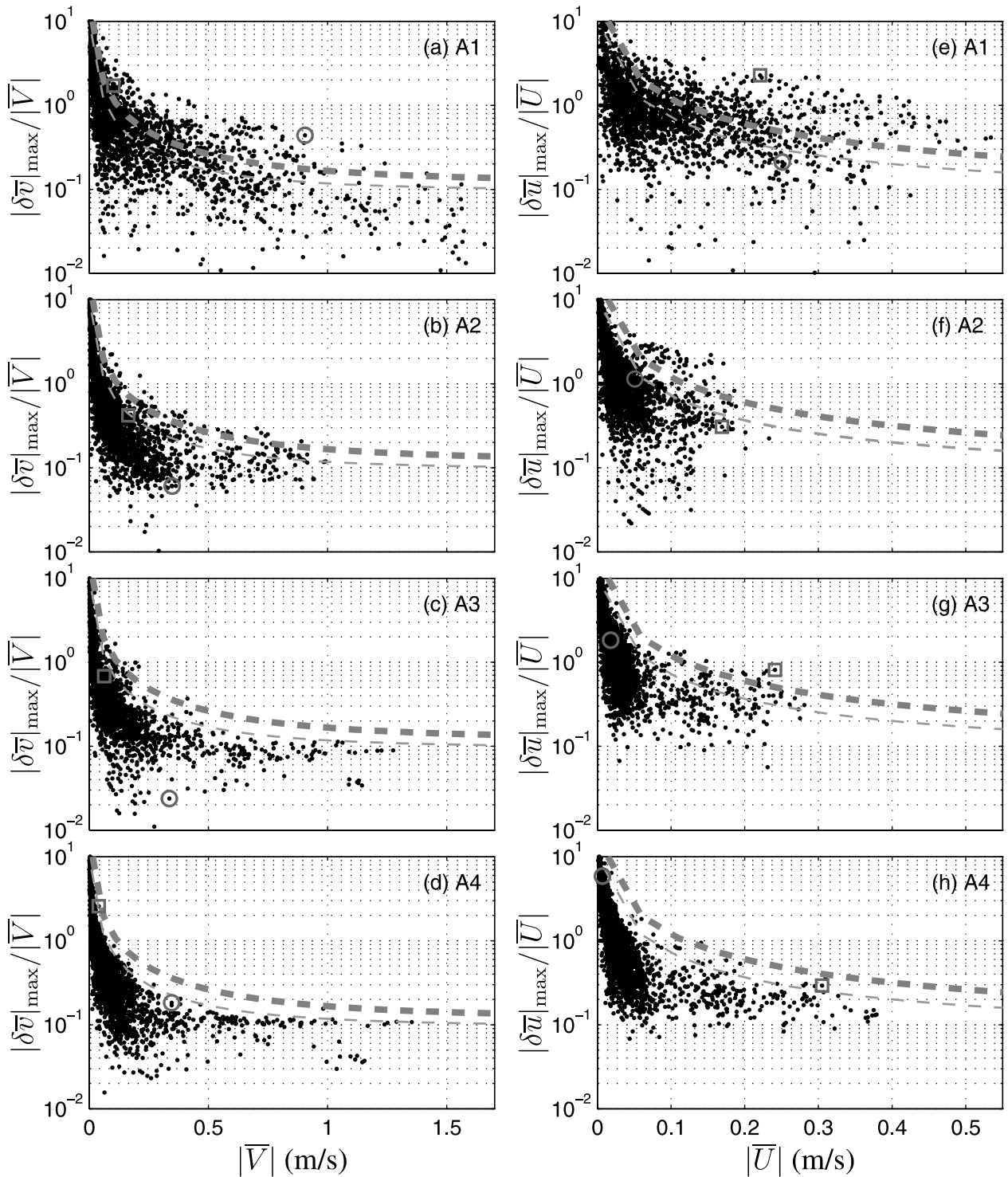


Figure 5. The ratio $|\delta\bar{v}|_{\max}/|\bar{v}|$ versus $|\bar{v}|$ (left column a–d) and the $|\delta\bar{u}|_{\max}/|\bar{u}|$ versus $|\bar{u}|$ (right column e–h) for alongshore transects A1 (top panel) to A4 (bottom panel). The A5 transect (not shown) is similar to A4. The 95% confidence levels for the N1 (upper, thick dashed) and N2 (lower, thin-dashed) current-meter noise models (Appendix C) are shown. An observation is shown only if at least three current meters are active on a transect, resulting in between 2007 (A1) and 2565 (A3) estimates out of 2664 possible. Note the different scales for \bar{v} and \bar{u} . The circles and squares in a–j correspond to the cases shown in Figure 6 (4 September) and 8 (14 November), respectively.

Table 3. Percentage of Time $|\delta\bar{v}|_{\max}/|\bar{v}|$ and $|\delta\bar{u}|_{\max}/|\bar{U}|$ That Exceed the N1 and N2 Current-Meter Noise Thresholds (Figure 5) for $|\bar{v}| > 0.1$ m/s and $|\bar{U}| > 0.1$ m/s

	A1, %	A2, %	A3, %	A4, %	A5, %
<i>Alongshore Current \bar{v}</i>					
N1	25	4	1	0	0
N2	47	18	5	1	1
<i>Cross-Shore Current \bar{u}</i>					
N1	33	16	8	1	0
N2	54	30	35	8	4

0.92 m on A2. No bathymetry survey data were available on this day, and the A1 \bar{v} nonuniformity was not observed two days later when a survey was performed. The cause for this \bar{v} nonuniformity at A1 is not known, but may possibly result from bathymetric nonuniformities located outside the measurement region.

4.2. Cross-Shore Current

[22] The interpretation of the deviation metric $|\delta\bar{u}|_{\max}/|\bar{U}|$ is less straightforward than the interpretation of $|\delta\bar{v}|_{\max}/|\bar{v}|$, because \bar{u} typically has more vertical shear [e.g., *Garcez-Faria et al.*, 1998] than \bar{v} [e.g., *Garcez-Faria et al.*, 2000]. Even with alongshore uniform cross-shore currents, the different current-meter elevations (0.4–1.0 m above the bottom) within an alongshore transect could result in substantial $|\delta\bar{u}|_{\max}$ that are interpreted as alongshore nonuniformity. Nevertheless, the same nonuniformity metric and noise models are used for \bar{u} and \bar{v} .

[23] In general, the magnitude of \bar{u} was much less than \bar{v} , but the pattern of the nonuniformity from onshore to offshore transects is similar (compare the right \bar{u} and left \bar{v} columns in Figure 5). At A1, \bar{u} nonuniformity often exceeded that expected from current-meter noise alone for all $|\bar{U}|$ (Figure 5e; Table 3). This transect had the largest $|\bar{U}|$ range, reaching 0.54 m/s, and 38% of the time $|\bar{U}| > 0.1$ m/s. At A1, 92% of the time $|\bar{U}| > 0$ (offshore directed), and the strongest $|\bar{U}| (>0.1$ m/s) all were directed offshore. Offshore \bar{U} also was prevalent at the other alongshore transects. At A2, $|\bar{U}|$ was weaker than the other transects (Figure 5f), similar to $|\bar{v}|$ at A2. For the 6% of the time when $|\bar{U}| > 0.1$ m/s, $|\delta\bar{u}|_{\max}/|\bar{U}|$ at times exceeded the noise thresholds but not as consistently as at A1 (Table 3). Farther offshore at A3–A5, $|\bar{U}|$ reached 0.38 m/s, but 85% of the time was ≤ 0.05 m/s (Figures 5g–5h), and \bar{u} was mostly alongshore uniform (Figures 5g–5h; Table 3).

[24] The circulation example (Figure 6) is typical of the alongshore uniform \bar{u} in Figure 5. At A1, the cross-shore currents were relatively strong ($|\bar{U}| = 0.25$ m/s), but $|\delta\bar{u}|_{\max}/|\bar{U}|$ did not exceed either noise threshold (circle in Figure 5e). At A2, \bar{u} was much reduced ($|\bar{U}| = 0.05$ m/s) and is uniform (circle in Figure 5f). At A3–A5, \bar{u} is small ($|\bar{U}| < 0.02$ m/s) and uniform.

4.3. Relationship of Bathymetric and Current Nonuniformities

[25] The circulation and bathymetric nonuniformities are both maximum at A1. However, no relationship is evident between \bar{v} and bathymetric nonuniformity. In particular, $|\delta\bar{v}|_{\max}$ is not correlated with γ^2 ($|r| = 0.03$, Figure 7) or

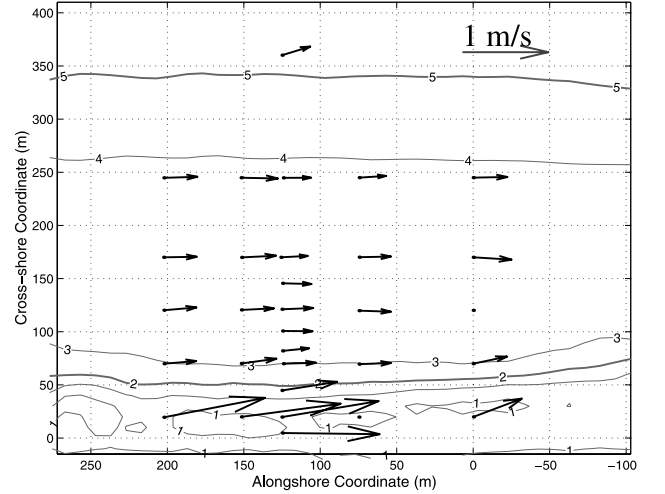


Figure 6. Mean circulation on 4 September (day 32) 1800–1900 EST. In 8-m depth $H_{\text{rms}} = 1.0$ m and $\theta = 30^\circ$. The maximum mean current speed was 1.1 m/s. Wind was alongshore at 10.3 m/s. Wave-breaking occurred onshore of $x = 70$ m (at A2). Bathymetry from 6 September (day 34) is contoured in units of meters below mean sea level. Circulation observations from additional locations not shown in Figure 1 are included.

with σ_h (not shown), and the ratio $|\delta\bar{v}|_{\max}/|\bar{v}|$ is not correlated with either γ^2 or σ_h (not shown). The correlation is also low between cross-shore current ($|\delta\bar{u}|_{\max}/|\bar{U}|$ or $|\delta\bar{u}|_{\max}$) and bathymetric nonuniformities at A1 (not shown), and also between circulation (both u and v) and bathymetric nonuniformities at A2. This is counter-intuitive to the expectation that bathymetric nonuniformities cause circulation nonuniformities, and no simple metric for predicting circulation nonuniformities based on local bathymetric nonuniformities was found. The \bar{v} nonuniformity may be due to bathymetric or wave nonuniformities located outside the measurement region. The circulation example (Figure 6) illustrates the lack of relationship between \bar{v} and local

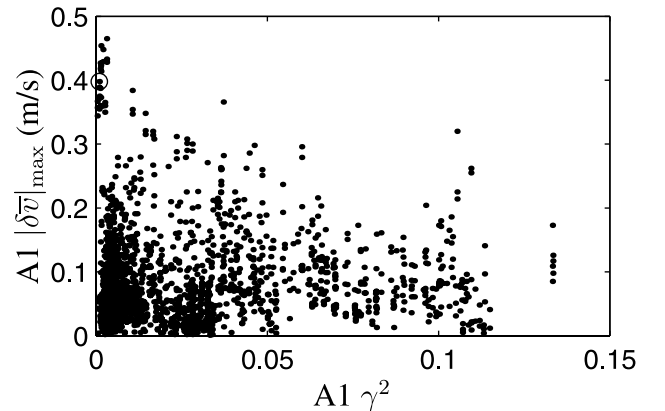


Figure 7. Maximum deviation $|\delta\bar{v}|_{\max}$ from the transect-averaged \bar{v} versus the bathymetric nonuniformity $\gamma^2(4)$ at A1. The circle (at $\gamma^2 \approx 0$ and $|\delta\bar{v}|_{\max} \approx 0.4$ m/s) corresponds to the case in Figure 6.

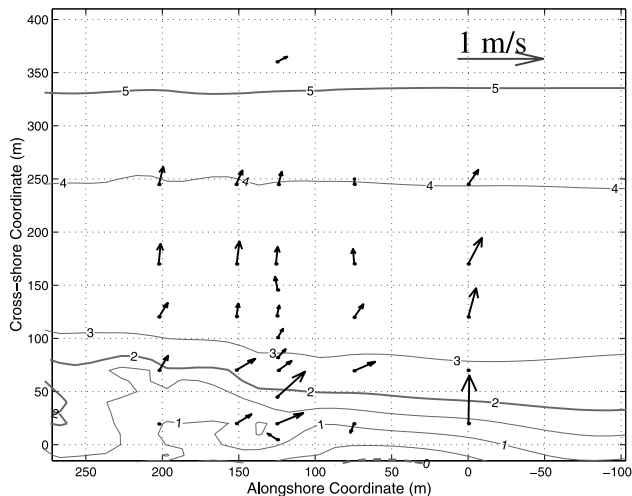


Figure 8. Mean circulation on 14 November (day 103) 0200–0300 EST, suggesting a rip current at $y = 0$ m. In 8-m depth $H_{rms} = 1.5$ m and $\theta = 0^\circ$. The maximum mean current speed was 0.72 m/s. The winds were weak at 3.1 m/s. Wave-breaking began at $x = 170$ m (A4). The contoured bathymetry is based on the survey of 11 November (day 100) and altimeter data from this one-hour period. Circulation observations from additional locations not shown in Figure 1 are included.

bathymetric nonuniformities (circle in Figure 7). There is significant \bar{v} nonuniformity (Figure 5a) with $|\delta\bar{v}|_{max} = 0.4$ m/s, but small A1 bathymetric nonuniformity ($\gamma^2 = 10^{-3}$ and $\sigma_h = 0.037$ m). Most of the points in Figure 7 with $0.35 < |\delta\bar{v}|_{max} < 0.47$ m/s and $\gamma^2 < 0.004$ occurred within 24 hours of Figure 6.

4.4. Rip Currents

[26] Rip currents were identified as coherently and significantly elevated (at the same alongshore location) $|\delta\bar{u}|_{max}/|\bar{U}|$ together with $\bar{U} > 0.1$ m/s extending from A1 to at least as far offshore as A2. Over the 2664 hours of data, including 620 hours when the offshore wave height exceeded 1 m, the alongshore locations of elevated $|\delta\bar{u}|_{max}/|\bar{U}|$ at A1 (Figure 5e) do not correspond to elevated $|\delta\bar{u}|_{max}/|\bar{U}|$ at A2 or A3, with one exception (Figure 8). Large, normally incident waves began breaking at A4 (260 m from the shore) driving a strong cross-shore current ($0.17 \leq |\bar{U}| \leq 0.31$ m/s) but small \bar{v} at all transects. At the southern end ($y = 0$ m) of A1, A3, and A4 (the A2 current-meter was inactive), \bar{u} is elevated relative to the mean corresponding to the elevated $|\delta\bar{u}|_{max}/|\bar{U}|$ (squares in Figures 5e–5h). At the southern end of A1, $\bar{u} = 0.72$ m/s, more than 0.5 m/s larger than $|\bar{u}|$ at the other A1 current-meters, and $|\delta\bar{u}|_{max}/|\bar{U}| = 2.28$, exceeding the noise thresholds. At A3, $|\bar{u}|$ at $y = 0$ is 0.2 m/s larger than any other A3 current-meter, and $|\delta\bar{u}|_{max}/|\bar{U}| = 0.81$ also exceeding the noise thresholds.

[27] This rip current was only observed for two hours when the mean wave direction was near normal incidence ($\theta < 0.5^\circ$ and $|S_{yx}|/\rho < 0.06$ m³/s²). At this time, $|\bar{v}|$ was weak (< 0.05 m/s) at A3 and A4. However, just before and shortly after these two hours, $|\theta|$ was larger and $|\bar{v}|$ at A3 and A4

was approximately 0.1 m/s. During the experiment, in 8-m depth the mean wave angle $|\theta| < 3^\circ$ only 7% of the time, and rarely for more than two consecutive hours. Numerical rip current experiments suggest that the offshore extent of rip currents is significantly reduced for (monochromatic) obliquely incident waves (deep water $|\theta| \geq 3^\circ$) and nonzero \bar{v} [Svendsen *et al.*, 2000; Yu and Slinn, 2002]. Persistent obliquely incident waves may be the reason that rip currents spanning several alongshore transects rarely were observed. The magnitude of rip currents observed at the near bottom current-meters also may be reduced because rip currents offshore of the surfzone are surface intensified [Haas and Svendsen, 2002] and meander spatially [Haller and Dalrymple, 2001]. Even though the array is not optimal for detecting them, the lack of observed rip currents spanning several alongshore transects during the experiment period is striking.

5. Summary

[28] The alongshore uniform (1-D) assumption for nearshore circulation is tested with 4 months of field observations on a natural beach. Cross-shore integrated alongshore momentum balances close with high skill ($r^2 \geq 0.87$) on five cross-shore transects, and the inferred c_d are alongshore uniform, demonstrating that the 1-D assumption for the alongshore current dynamics is valid. The alongshore uniformity of the circulation is investigated kinematically at several cross-shore locations. Except close to the shoreline (≈ 1 m depth), the mean cross- and alongshore current was alongshore uniform, with deviations from uniformity no larger than expected from current-meter noise, and the bathymetric nonuniformities were also small. Close to the shoreline at A1, there could be significant circulation and bathymetric nonuniformity, but counter to expectations, no relationship between bathymetric nonuniformities and circulation nonuniformities was found. Rip currents that extended more than 75 m offshore rarely were observed.

[29] The alongshore uniform circulation, inferred both dynamically and kinematically, implies that the alongshore current dynamics can be represented by the 1-D dynamics (1), and that a model that correctly parameterizes the wave-forcing, lateral mixing, and bottom stress processes can accurately predict the alongshore current.

Appendix A: Interpretation of Best Fit c_d

[30] The drag coefficient c_d is passed through the bottom stress integral in (6) even though c_d likely is not constant in the cross-shore direction. However, the resulting best fit c_d can be interpreted as a cross-shore averaged c_d . The ‘‘First Mean Value Theorem’’ [Gradshteyn and Ryzhik, 1965] states: Let $f(x)$ and $g(x)$ be two bounded functions, integrable in $[a, b]$ and let $g(x)$ be of one sign in this interval. Then

$$\int_a^b f(x)g(x)dx = f(c) \int_a^b g(x)dx$$

with $a \leq c \leq b$. Applying this to the cross-shore bottom stress integral $\int_0^x c_d \langle |\bar{u}|v \rangle dx$, let $g(x) = \langle |\bar{u}|v \rangle$ and $f(x) = c_d(x)$. This decomposition is valid because $\langle |\bar{u}|v \rangle$ (or \bar{v})

rarely changes sign across the nearshore (Figure 6). Assuming that c_d is an integrable function with no singularities at the shoreline, then

$$\int_0^{x_s} c_d(x) \langle |\bar{u}|v \rangle dx = c_d(x_a) \int_0^{x_s} \langle |\bar{u}|v \rangle dx$$

where x_a is a cross-shore location between the shoreline and the offshore end of the transect. Thus the best fit c_d can be interpreted as a weighted transect average c_d .

Appendix B: Integration and Least Squares Methods

[31] Hourly cross-shore integrals such as $\int_0^{x_s} \langle |\bar{u}|v \rangle dx$ where $x = 0$ and $x = x_s$ represent the shoreline and the offshore end of cross-shore transect respectively, were estimated from observations using the trapezoidal rule. Cross-shore integrals are calculated only if all five transect instruments are active during the particular hour, resulting in significantly fewer hourly integrals than the 2664 total hours of the experiment (Table 2). Low tide data were often excluded because sensors on the shallowest alongshore transect A1 were not submerged. On the cross-shore transects, the most nearshore sensor is used as a proxy for the shoreline (Figure 1). At high tides, this location can be up to 20 m offshore of the mean shoreline. Therefore, these integrals may have a bias toward reduced magnitudes, which could positively bias the best fit c_d estimates. The integrated acceleration term (7) was estimated by time differencing successive hourly transport integral ($\int_0^{x_s} h\bar{v}dx$) estimates on the same transect. The nonlinear advection term (8) was calculated by differencing $\int_0^{x_s} h\bar{v}^2 dx$ estimates between various alongshore locations.

[32] The linear regression to estimate the drag coefficient c_d and uncertainty σ_{c_d} assumes a noise level of $\sigma_n = 0.1 \text{ m}^3/\text{s}^2$ and a noise decorrelation timescale $T_n = 2$ hours. Regressions using an a priori zero mean or an estimated mean yield similar results. Most measures of T_n (integral timescale [Davis, 1976]) result in $T_n \approx 12$ hours. However, this assumes a Gaussian process, whereas statistics of the observed residuals are not Gaussian. Using $T_n = 12$ hours results in significant degradation of fit due to smoothing of rapid forcing events, and thus in underestimation of c_d . The RMS residual to the fit ($\approx 0.05 \text{ m}^3/\text{s}^2$) also are smaller than the assumed noise level $\sigma_n = 0.1 \text{ m}^3/\text{s}^2$, however the assumed σ_n is more consistent with higher norms (that are more appropriate for non-Gaussian processes) of the residuals. For these reasons, the estimated σ_{c_d} are qualitative.

Appendix C: Current-Meter Noise Models

[33] Current-meter noise is modeled as the sum of two independent components, an offset error (velocity measured with no fluid motion) and a gain error proportional to the current magnitude. The following discussion refers to \bar{v} , but also applies to \bar{u} . The offset error is assumed to be a zero-mean Gaussian random variable with standard deviation σ_{off} . The gain error is assumed to be a zero-mean Gaussian random variable, linear in \bar{v} , with standard deviation $\sigma_g = \alpha\bar{v}$, where α is the fractional gain error.

The total current-meter noise, the sum of these two random variables, is a zero-mean Gaussian random variable with standard deviation

$$\sigma_{\text{cm}} = \left(\sigma_{\text{off}}^2 + (\alpha\bar{v})^2 \right)^{1/2}. \quad (\text{C1})$$

[34] Two noise thresholds are calculated from this noise model. The first, denoted N1, uses $\sigma_{\text{off}} = 5 \text{ cm/s}$, conservatively based on in situ current-meter rotations during periods of weak flow and gain error of 5% ($\alpha = 0.05$) based on laboratory calibrations. The second noise threshold, denoted N2, follows from assuming that \bar{v} observed at A4 and A5 are truly alongshore uniform, and fitting σ_{off} and α to the observed $|\delta\bar{v}|_{\text{max}}/|\bar{v}|$. The resulting $\sigma_{\text{off}} = 3 \text{ cm/s}$ and $\alpha = 0.04$ are reductions from the N1 current-meter noise levels, suggesting that the N1 noise levels are overestimated at A4 and A5. However, it is not clear whether the N2 noise model is applicable farther inshore.

[35] The 95% alongshore uniform threshold curves in Figure 5 are used to test the hypothesis that \bar{v} on an alongshore transect are uniform given the expected current-meter noise levels (C1). For this test, the alongshore averaged \bar{v} is assumed to be the true alongshore uniform \bar{v} , and is used in the bias error component of σ_{cm} . If \bar{v} truly is alongshore uniform, then the deviations from the mean $\bar{v}(\delta\bar{v})$ are due solely to current-meter noise and are thus zero-mean Gaussian random variables with standard deviation σ_{cm} . The $\delta\bar{v}$ are only calculated when at least three current-meters are active on an alongshore transect. With three independent random Gaussian variable samples, there is only a 5% probability that $|\delta\bar{v}|_{\text{max}}/|\bar{v}| \geq 2.35\sigma_{\text{cm}}/|\bar{v}|$ which represents the noise threshold line in Figure 5.

[36] If the processes governing \bar{v} (waves, wind, and bathymetry) were stationary, then the following statistical test can be applied: If greater than 5% of $|\delta\bar{v}|_{\text{max}}/|\bar{v}|$ exceed this threshold, then the hypothesis that \bar{v} is alongshore uniform fails. However, the governing processes are not stationary, and thus such a statistical test cannot be rigorously applied. The noise threshold curves in Figure 5 are useful in qualitatively determining whether the observed nonuniformity exceeds that expected from current-meter noise alone.

[37] **Acknowledgments.** This research was supported by the Office of Naval Research and the National Ocean Partnership Program. The surfzone sensor array was constructed, deployed, and maintained by staff from the Center for Coastal Studies. Steve Elgar and Britt Raubenheimer helped design and manage the field experiment, and provided high quality data. The Field Research Facility, Coastal Engineering Research Center, Duck, N. C., provided excellent logistical support, the bathymetric surveys, and the 8m-depth pressure array data. Tom Herbers processed the 8-m array data. We thank Steve Elgar, Rob Holman, Steve Lentz, and John Trowbridge for helpful discussions. Woods Hole Oceanographic Institution contribution 10,594.

References

- Church, J. C., and E. B. Thornton, Effects of breaking wave induced turbulence within a longshore current model, *Coastal Eng.*, 20, 1–28, 1993.
- Davis, R. E., Predictability of sea surface temperature and sea level pressure anomalies over the North Pacific Ocean, *J. Phys. Oceanogr.*, 6, 249–266, 1976.
- Elgar, S., T. H. C. Herbers, and R. T. Guza, Reflection of ocean surface gravity waves from a natural beach, *J. Phys. Oceanogr.*, 24, 1503–1511, 1994.
- Elgar, S., R. T. Guza, W. C. O'Reilly, B. Raubenheimer, and T. H. C. Herbers, Wave energy and direction observed near a pier, *J. Waterw. Port Coastal Ocean Eng.*, 127, 2–6, 2001.

- Feddersen, F., R. T. Guza, S. Elgar, and T. H. C. Herbers, Cross-shore structure of longshore currents during Duck94, in *Proceedings of the 25th International Coastal Engineering Conference*, pp. 3666–3679, Am. Soc. of Civ. Eng., New York, 1996.
- Feddersen, F., R. T. Guza, S. Elgar, and T. H. C. Herbers, Alongshore momentum balances in the nearshore, *J. Geophys. Res.*, *103*, 15,667–15,676, 1998.
- Garcez-Faria, A. F., E. B. Thornton, T. P. Stanton, C. M. Soares, and T. C. Lippmann, Vertical profiles of longshore currents and related bed shear stress and bottom roughness, *J. Geophys. Res.*, *103*, 3217–3232, 1998.
- Garcez-Faria, A. F., E. B. Thornton, T. C. Lippmann, and T. P. Stanton, Undertow over a barred beach, *J. Geophys. Res.*, *105*, 16,999–17,010, 2000.
- Gradshteyn, I. S., and I. M. Ryzhik, *Table of Integrals, Series, and Products*, Academic, San Diego, Calif., 1965.
- Haas, K. A., and I. A. Svendsen, Laboratory measurements of the vertical structure of rip currents, *J. Geophys. Res.*, *107*, 3047, 10.1029/2001JC000911, 2002.
- Haller, M. C., and R. A. Dalrymple, Rip current instabilities, *J. Fluid Mech.*, *433*, 161–192, 2001.
- Large, W. G., and S. Pond, Open ocean momentum flux measurements in moderate to strong winds, *J. Phys. Oceanogr.*, *11*, 324–336, 1981.
- Lentz, S. J., R. T. Guza, S. Elgar, F. Feddersen, and T. H. C. Herbers, Momentum balances on the North Carolina inner shelf, *J. Geophys. Res.*, *104*, 18,205–18,226, 1999.
- Long, C. E., Index and bulk parameters for frequency-direction spectra measured at CERC Field Research Facility, June 1994 to August 1995, *Misc. Pap. CERC-96-6*, U.S. Army Eng. Waterw. Exp. Stn., Vicksburg, Miss., 1996.
- Longuet-Higgins, M. S., Longshore currents generated by obliquely incident sea waves 1, *J. Geophys. Res.*, *75*, 6790–6801, 1970.
- Reniers, A., E. B. Thornton, and T. C. Lippmann, Longshore currents over barred beaches, in *Coastal Dynamics '95*, pp. 413–424, Am. Soc. of Civ. Eng., New York, 1995.
- Ruessink, B. G., J. R. Miles, F. Feddersen, R. T. Guza, and S. Elgar, Modeling the alongshore current on barred beaches, *J. Geophys. Res.*, *106*, 22,451–22,463, 2001.
- Svendsen, I. A., K. Haas, and Q. Zhao, Analysis of rip current systems, in *Proceedings of the 27th International Conference on Coastal Engineering*, pp. 1127–1140, Am. Soc. of Civ. Eng., New York, 2000.
- Thornton, E. B., and R. T. Guza, Surf zone longshore currents and random waves: Field data and models, *J. Phys. Oceanogr.*, *16*, 1165–1178, 1986.
- Yu, J., and D. N. Slinn, Effects of wave-current interaction on rip currents, *J. Geophys. Res.*, *107*, doi:10.1029/2001JC001105, in press, 2002.

F. Feddersen, Woods Hole Oceanographic Institution, Woods Hole, MA 02543, USA. (falk@whoi.edu)

R. T. Guza, Scripps Institution of Oceanography, University of California, La Jolla, CA 92093-0209, USA. (rguza@ucsd.edu)